Operational Cloud Boundary Detection and Analysis from Micropulse Lidar Data

J. R. Campbell and D. L. Hlavka
Science Systems and Applications Inc.
Greenbelt, Maryland

J. D. Spinhirne
NASA-Goddard Space Flight Center
Greenbelt, Maryland

D. D. Turner and C. J. Flynn
Pacific Northwest National Laboratory
Richland, Washington

Introduction

The micropulse lidar (MPL) was developed at the National Aeronautics and Space Administration's (NASA's) Goddard Space Flight Center (GSFC) as the result of research on space-borne lidar techniques. It was designed to provide continuous, unattended observations of all significant atmospheric cloud and aerosol structure with a rugged, compact system design and the benefit of eye safety (Spinhirne 1993). The significant eye safety feature is achieved by using low pulse energies and high pulse repetition rates compared to standard lidar systems. MPL systems use a diode-pumped 10 μj, 2500-Hz doubled Nd:YLF laser. In addition, a solid-state Geiger mode avalanche photo diode (GAPD) photon counting detector is used allowing for quantum efficiencies approaching 70%. Other design features have previously been noted by Spinhirne et al. (1995).

MPL data can be used to yield numerous cloud radiative and physical parameters, including cloud boundary heights to the limit of signal attenuation, cloud scattering cross sections and optical thicknesses, planetary boundary layer heights and aerosol scattering profiles, including those into the stratosphere in nighttime cases (Hlavka et al. 1997). MPL vertical resolution ranges from 30 m to 300 m (i.e., high and low resolution, respectively) depending on system design.

Three MPL units have been operated by the Atmospheric Radiation Measurement (ARM) Program over the past 4 years. At the Southern Great Plains (SGP) Cloud and Radiation Testbed (CART) site, a prototype system (MPL000) was first installed in December 1993. A system upgrade (MPL002) followed in January 1996 improving data quality through an increase in signal strength by a factor of nearly 10. This system remains there to this day. At the Tropical Western Pacific (TWP) Atmospheric Radiation and Cloud Station (ARCS) on Manus Island, a low resolution unit (MPL003) began operating in February 1997. Though this system suffered through laser diode degradation over the fall of that year, ongoing maintenance should make it operable by the summer of 1998. High resolution systems will soon come online at the North Slope of Alaska (NSA) CART and TWP ARCS-II sites, providing the exciting prospect of more extensive datasets.

Data Processing

MPL systems record 1-minute shot averages in one of three possible byte arrays, depending on system and vertical resolution. The prototype instrument used a byte length of 825, low resolution systems use 836, and high resolution systems will use 8048. From the lidar equation, raw count rates take the form

$$n(r) = \frac{\dfrac{\left(O_c(r)CE\beta(r)T^2\right)}{r^2} + n_b + n_{ap}(r)}{DTC[n(r)]} \tag{1}$$

where:

- n = the measured signal return in photo electron counts per second at range r
- O_c = the overlap correction as a function of range caused by field of view conflicts in the transmitter-receiver system
- C = a dimensional system calibration constant
- E = the transmitted laser pulse energy

β = the backscatter cross section due to all types of atmospheric scattering
T = atmospheric transmittance
n_b = background contribution from ambient light
n_{ap} = the afterpulse correction for detector run on
DTC = the detector offset deadtime correction as a function of raw count rate.

In conjunction with the ARM Data Center, a processing algorithm developed at GSFC has been added to the ARM value added procedure (VAP) code, which takes equation (1) to the form:

$$\frac{\left[\left[n(r) * DTC[n(r)]\right] - n_b - n_{ap}(r)\right] r^2}{O_c(r)E} = C\beta(r)T^2 \qquad (2)$$

This product is referred to as normalized relative backscatter (NRB). Dividing C through the left-hand side of this equation yields attenuated backscatter. But this task is left to data users as C must be solved for on a case-by-case basis.

Solving for Eq. (2) requires calibrating each MPL for signal and range-dependent deadtime, afterpulse, and overlap corrections. Deadtime corrections are provided as a function of raw count rate by the photon detector manufacturer. A curve-fit equation is fit to these specifications for use in the VAP code. Overlap correction is produced by recording an extended period of data with the MPL where aerosol backscatter is constant with distance (i.e., horizontally aimed profile where target aerosol layer is assumed homogeneous). Implicitly at some range, r_o, the overlap ceases to exist and the correction factor becomes 1.0. Eq. (1) can be written as:

$$\begin{aligned} P(r) &= \left[\left(n(r) * DTC\left[n(r)\right]\right) - n_b - n_{ap}(r)\right] r^2 \\ &= O_c(r) CE\beta(r) T^2 \end{aligned} \qquad (3)$$

Knowing that $T = e^{-\tau}$ and $\tau = \sigma r$, where τ is the optical thickness through the layer and σ is the extinction cross section, Eq. (3) can be rewritten as:

$$P(r) = O_c(r) CE\beta(r) e^{-2r\sigma} \qquad (4)$$

For the section of this function where $r > r_o$ and $O_c = 1.0$, taking the natural log of both sides of Eq. (4) yields:

$$\ln\left[P(r)\right] = \ln\left[CE\beta(r)\right] - 2r\sigma \qquad (5)$$

Because this layer is assumed homogeneous, $CE\beta$ becomes constant. Plotting ln[P] versus r takes the form of y = mx + b with -2σ as the slope m. Fitting a line to the points where $r > r_o$, as in Figure 1, and calculating the slope value, Eq. (4) can be solved for O_c as:

$$O_c(r) = \frac{P(r)}{CE\beta(r) e^{-2r\sigma}} \qquad (6)$$

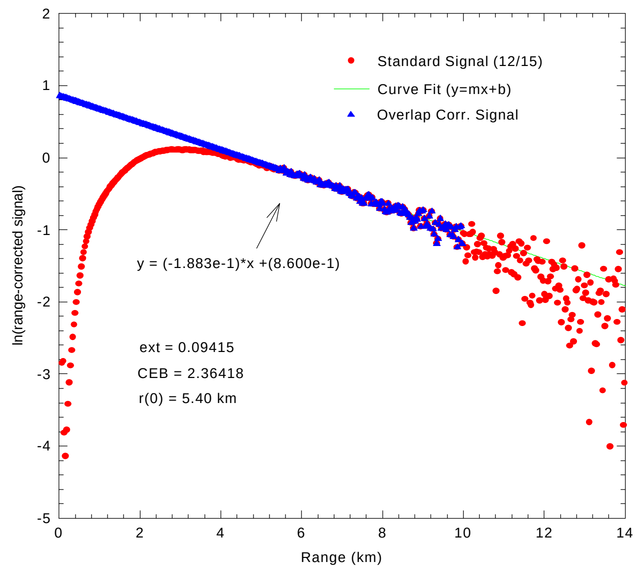

Figure 1. Overlap correction development. (For a color version of this figure, please see *http://www.arm.gov/docs/documents/technical/conf_9803/campbell-98.pdf*.)

However, since $CE\beta$ is a constant, we can solve for it with Eq. (5), where $r > r_o$ and $O_c = 1.0$, and plug this value into Eq. (6) to solve for the overlap correction as a function of range. The afterpulse correction is developed, taking data while pointing the system at a hard target, preferably 300 m in range. By blocking the laser pulse, detector readings past the target range yield the residual afterpulse signature. Once again, a curve-fit equation is developed to this function and used in Eq. (1).

Cloud Boundary Height Algorithm

The GSFC cloud boundary height algorithm developed for ARM VAP processing, uses bi-directional vertical differencing of adjacent range bins from 1-minute shot averages compared to a similarly analyzed clear-sky baseline profile. Differences between the two may then be analyzed for possible cloud boundaries. Days are divided into 12 separate analyzing periods from which averaged shots can be examined for both possible baseline inclusion and cloud boundary search. The cloud threshold is a combination of a relative signal and signal-to-noise ratio (SNR) increase, varying upon observed background count rates.

For each averaged shot, a running three-point sum of the derivative of the natural log of NRB is taken vertically from the first data range bin to areas of deviance, whereby any bin summing over 1.0 is thought to possess cloud. This process discriminates between clear and cloudy shots within a period to produce baseline updates. A varying minimum of clear shots, based on locale, is required to produce baseline updates. Additionally, as larger variations in signal structure take place in the boundary layer on the scale of 2 hours (one period), the section of the baseline below 3 km can be updated irrespective of the remainder if the minimum clear shot standard is reached amongst its region. Therefore, despite cases of prolonged high cloudiness, the boundary layer section of the baseline continues to update. A linear bridge is built between the two sections to smooth out any discontinuities in relative signal differencing, which may occur. The baseline consists of NRB and SNR averages for each bin. SNR is obtained by reverting NRB back to raw count rates as

$$\mathrm{SNR}(r) = \frac{\dfrac{N(r)O_c(r)N_sE}{r^2}}{\sqrt{\dfrac{N(r)O_c(r)N_sE}{r^2} + B_sN_s}} \qquad (7)$$

where:

N = NRB as a function of range
N_s = the number of shots in a 1-minute average (normally 150,000)
B_s = the solar background count.

Figure 2 displays algorithm output for the first 2 km of a shot average taken by the MPL003. The first column refers to the height above ground level (AGL) of the center of the corresponding range bin and the second notes the NRB value recorded for that bin. The third column is the percentage increase of backscatter between the bin below and the subject bin, with the same calculation from the bin above to the subject bin listed below. The fourth column is the same process done for the clear-sky baseline, and the fifth column is the cumulative difference between the

HGHT	BS	BSDF	BADF	DIFF	SNR	SNDF	BSND	DIFF	CLD	SPK
0.27	0.609	1.665	0	1.665	763.06	0.546	0	0.546	Base	yes
		-0.333	0.149	-0.481		0.261	0.605	-0.344		no
0.57	0.913	0.499	-0.129	0.628	605.04	-0.207	-0.377	0.17	Mid	yes
		-0.143	-0.037	-0.106		0.115	0.167	-0.053		no
0.87	1.065	0.167	0.039	0.128	542.79	-0.103	-0.143	0.04	Mid	no
		0.447	-0.043	0.49		0.503	0.132	0.371		yes
1.17	0.736	-0.309	0.045	-0.354	361.24	-0.334	-0.116	-0.218	Top	no
		0.591	-0.052	0.643		0.637	0.109	0.528		yes
1.47	0.462	-0.372	0.055	-0.426	220.72	-0.389	-0.098	-0.291	n/a	no
		0.351	0.018	0.333		0.489	0.138	0.351		no
1.77	0.342	-0.26	-0.018	-0.242	148.27	-0.328	-0.121	-0.207	n/a	no
		0.344	0.174	0.17		0.502	0.213	0.289		no
2.07	0.255	-0.256	-0.148	-0.108	98.71	-0.334	-0.176	-0.158	n/a	no
		0.247	0.34	-0.093		0.418	0.265	0.152		no

Figure 2. Cloud boundary detection algorithm statistical output for the first 2 km of a shot average.

values. Note that the first and last bin (not shown) use the baseline value to calculate upward and downward increases, respectively. The next four columns show the same process for SNR values. The final two columns contain cloud boundary markers and the direction of signal spikes responsible for them, respectively.

For a cloud boundary to be observed, a one- or two-bin relative NRB increase (either upward of downward) of at least 55% and an SNR increase greater than approximately 42% (the number becomes slightly less near the ground) is required. Because this relationship is not fixed due to variance in solar background rates, requiring both increases results in an elastic threshold. For example, during daytime, where background values are relatively high, a 55% increase in NRB corresponds to an SNR increase of well over 42%. However, at night where background rates are very low, a 55% increase in NRB corresponds to an SNR increase much less than required, thus demanding greater relative NRB increases (than 55%) for detecting cloud. Thus, the threshold becomes the NRB increase in cases of little noise and becomes the SNR increase when background rates are high.

Working upward from the base range bin once an "upspike" is detected (as in the 0.27 km bin on Figure 2), signaling an upwards relative increase in NRB and SNR meeting the threshold requirement, the algorithm sets a cloud base at the corresponding height. A "downspike" is then sought signaling the top of the cloud. While searching, the algorithm ignores other upspikes until a cloud top is found. Additionally, once a cloud top is conditionally found, the following bin above is examined in case of another downspike caused by a continued downtrend in signal strength marking the true cloud top. Figure 3 plots NRB and cloud boundary height data for a cirrus layer observed on 23 January 1998 at SGP between 0400 Greenwich Mean

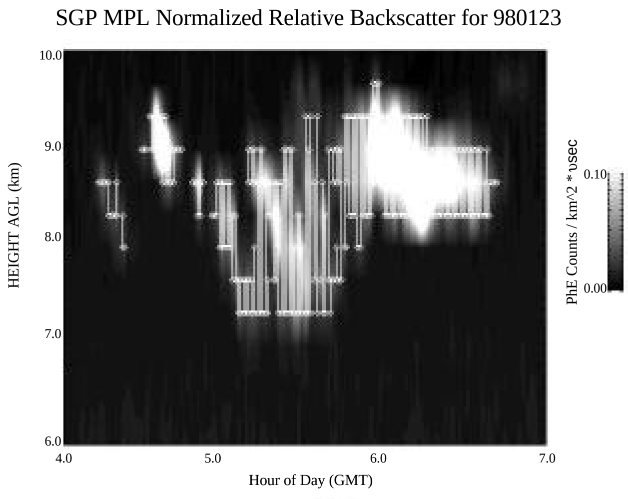

Figure 3. Cloud boundary algorithm heights superimposed on processed MPL data on 23 January 1998 between 0400 and 0700 GMT.

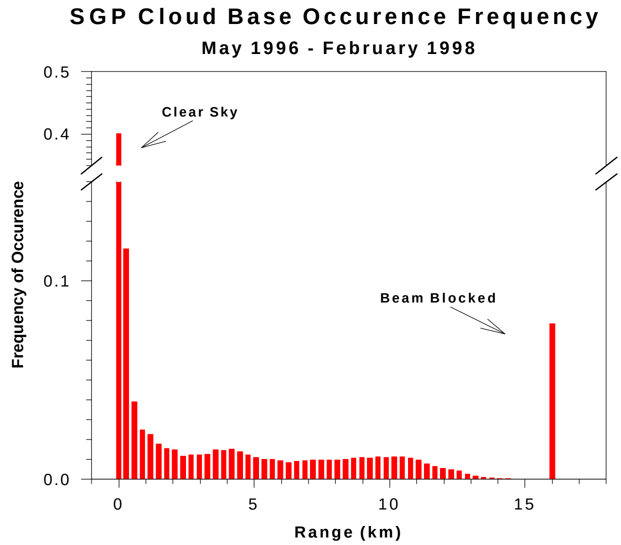

Figure 4. Cloud base range bin frequencies for MPL-SGP data between 5/96 and 2/98. For a color version of this figure, please see *http://www.arm.gov/docs/documents/technical/conf_9803/campbell-98.pdf*.)

Time (GMT) and 0700 GMT. Due to the coarse resolution of the currently operational MPLs, gaps between clouds of one range bin (i.e., 300 m) are smoothed requiring at least 600 m of separation between a cloud top and new base. The anticipated availability of processed high-resolution datasets in the near future will change this condition.

Climatological Statistics

Cloud base heights from processed MPL data between May 1996 and February 1998 at SGP were examined for range bin occurrence frequencies. Figure 4 shows these data. Future work will include supplementing these heights with linearly interpolated balloon sonde data recorded onsite.

The addition of parameters, including temperatures, pressures and wind data, will complement boundary heights in producing a complete cloud climatology for north central Oklahoma as well as for other ARM sites.

Summary

The data archive produced by ARM-owned MPL systems includes a combined total of over 4 years of nearly continuous observations from north-central Oklahoma and Manus Island, Papua New Guinea. Development within the ARM VAP code has yielded a real-time MPL data product providing normalized relative backscatter and multiple cloud boundary heights to the community. The inherent ability of lidar systems to yield many atmospheric radiative and physical properties placed great emphasis on the creation of such a product to realize the full potential of the MPL database. In particular, extensive cloud climatologies should result from these observations aiding in the knowledge of regional cloud variations.

Acknowledgments

The authors wish to thank Ms. Robin Perez (ARM) for her efforts in coordinating the extensive computer processing of the ARM MPL datasets and Mr. V. Stanley Scott III for his continued technical input on the instrument.

References

Hlavka, D. H., J. D. Spinhirne, V. S. Scott, A. E. Galbraith, and J. A. Reagan, 1997: Full time lidar cloud and aerosol height distribution data sets to support radiation/climate forcing studies. In *Abstracts of the 9th Conference on Atmospheric Radiation*, AMS, 1.15.

Spinhirne, J. D., 1993: Micro pulse lidar. *IEEE Trans. Geo. Rem. Sens.*, **31**, 48-55.

Spinhirne, J. D., J. A. R. Rall, and V. S. Scott, 1995: Compact eye safe lidar systems. *Rev. Laser Eng.*, **23**, 112-118.